



**HAL**  
open science

## LaFeO<sub>3</sub> thin films on Yttria Stabilized Zirconia flexible substrate

M. Jędrusik, Ch. Turquat, P. Eyméoud, A. Merlen, Madjid Arab, G. Cempura, L. Cieniek, A. Kopia, Ch. Leroux

► **To cite this version:**

M. Jędrusik, Ch. Turquat, P. Eyméoud, A. Merlen, Madjid Arab, et al.. LaFeO<sub>3</sub> thin films on Yttria Stabilized Zirconia flexible substrate. *Thin Solid Films*, 2023, 780, pp.139951. 10.1016/j.tsf.2023.139951 . hal-04290861

**HAL Id: hal-04290861**

**<https://hal.science/hal-04290861v1>**

Submitted on 19 Jul 2024

**HAL** is a multi-disciplinary open access archive for the deposit and dissemination of scientific research documents, whether they are published or not. The documents may come from teaching and research institutions in France or abroad, or from public or private research centers.

L'archive ouverte pluridisciplinaire **HAL**, est destinée au dépôt et à la diffusion de documents scientifiques de niveau recherche, publiés ou non, émanant des établissements d'enseignement et de recherche français ou étrangers, des laboratoires publics ou privés.

# LaFeO<sub>3</sub> thin films on YSZ flexible substrate

M. Jędrusik<sup>1,2</sup>, Ch. Turquat<sup>1</sup>, P. Eymeoud<sup>1</sup>, A. Merlen<sup>1</sup>, G. Cempura<sup>2</sup>, L. Cieniek<sup>2</sup>, A. Kopia<sup>2</sup>, Ch. Leroux<sup>\*1</sup>

<sup>1</sup> Université de Toulon, Aix Marseille Université, CNRS, IM2NP, Toulon, France

<sup>2</sup> Faculty of Metals Engineering and Industrial Computer Science, AGH University of Science and Technology, al. Mickiewicza 30, 30-059 Cracow, Poland

Corresponding author: leroux@univ-tln.fr

## Highlights :

- LaFeO<sub>3</sub> thin films were successfully grown on tetragonal flexible YSZ substrate for the first time
- The occurrence of vacancies in LaFeO<sub>3</sub> thin films was evidenced through Raman spectroscopy, as well as Chemi-Stem.
- LaFeO<sub>3</sub> thin films has two types of grain termination, flat or tip-like
- {112} twins in LaFeO<sub>3</sub> were observed as a consequence of the grain curvature of T-YSZ substrate.

## Abstract :

Thin films of LaFeO<sub>3</sub> were grown by pulsed laser deposition on a flexible tetragonal yttria stabilized zirconia substrate. Their structure and morphology were investigated using SEM, TEM, Chemi-STEM EDS, XRD and Raman Spectroscopy techniques. All grains of the polycrystalline substrate T-YSZ were covered by a homogeneous LaFeO<sub>3</sub> film, even at the grain boundaries. The thin films are 100 nm thick with nanocrystalline grains around 60 nm in lateral size. The chemical analyses show deficiency of Fe in the thin film. Atomic-scale microstructure investigations revealed twins in LaFeO<sub>3</sub> grains, as adaptation to the curvature of the T-YSZ grains. The main growth directions of the grains are [110] and [010]. Flat ended

---

and tip-like grains were observed, as in LaFeO<sub>3</sub> thin films deposited on silicon. The exposed facets are {110} or {010} for flat ended grains, {010} and {100} for tip-like termination.

This work shows the feasibility of covering flexible T-YSZ substrate with homogeneous perovskites thin films by PLD, that may be used for flexible sensing devices.

**Keywords:** LaFeO<sub>3</sub>, thin films, PLD, T-YSZ substrate

## 1. Introduction

The LaFeO<sub>3</sub> orthoferrite compound has been already reported for various applications, such as gas sensing, catalysis, photocatalysis, and solid oxides fuel cells. LaFeO<sub>3</sub> is a mixed ionic and electronic conductor (MIEC), is one of the most promising catalytic material for the production of hydrogen, by reduction of CO<sub>2</sub> [1], CH<sub>4</sub> [2], or by water splitting [3]. Due to a band gap of 2.6 eV, corresponding to a wavelength of 475 nm (blue light), the photocatalytic activity of LaFeO<sub>3</sub> under visible light was demonstrated, in case of degradation of organic pollutant [4], but also on the photoelectrochemical water splitting [5,6]. LaFeO<sub>3</sub> films were efficient in the detection of NO<sub>2</sub>, as sensing electrodes in electrochemical gas sensors [7] or in semi conducting metal oxide-based gas sensors [8]. Thick films of LaFeO<sub>3</sub> proved to be selective to acetylene in a gas mixture containing also CO, H<sub>2</sub>, and CO<sub>2</sub> [9]. Detection of formaldehyde at the ppb level could be realized with thin films of LaFeO<sub>3</sub> [10]. In recent works, depending on the application field, and the expected microstructure, several substrates on which the films are deposited were used. Epitaxial thin films were grown on SrTiO<sub>3</sub> [11], MgO [12], or GdScO<sub>3</sub> [13], when control of the interfaces or twin free films were needed. When seeking integration on micro electronic devices, LaFeO<sub>3</sub> thin films were grown on silicon [14, 15]. For devices implying charge carriers exchange between substrate and film, like in solid fuel cells or electrochemical sensors, yttria-stabilized zirconia (YSZ) is often used as substrate, because of its high ionic conductivity and low electronic conductivity at high temperature combined with chemical and crystallographic inertness over a wide range of temperature [16-18]. All these substrates are rigid, but it could be interesting to grow LaFeO<sub>3</sub> on flexible substrates. Indeed, there is a growing need of flexible sensing devices, able to adapt to various shapes, for applications that requires bending, or folding of the material [19]. Flexible layer of polymer composite with LaFeO<sub>3</sub> nanoparticles with high permittivity and low dielectric loss were recently elaborated [20]. Strain engineering leads to new properties for thin films grown on flexible substrates, as was recently demonstrated by Wu *et al.* in 2021 [21], in the case of flexoelectric LaFeO<sub>3</sub> photodetectors.

In this work, we selected tetragonal yttria stabilized zirconia (T-YSZ) as flexible substrate and used Pulsed Laser Deposition to grow thin films of  $\text{LaFeO}_3$  on it. This is the first time in literature that T-YSZ is reported as substrate for the direct growth of thin oxide films. Up to now, T-YSZ was barely used in literature as substrate for thick oxide films [22] or buffer layer for the growth of ZnO thin films on silicon [23]. Only recently, ultra-thin (20  $\mu\text{m}$ ) T-YSZ flexible substrates were investigated for infrared nano optics [24], T-YSZ tapes for their mechanical properties [25] and for their thermal conductivity [26]. T-YSZ was also used in SOFC instead of C-YSZ to improve the mechanical strength of the NiO-YSZ anode [27]. Two dimensional  $\text{MoS}_2$  semi-conductors were recently grown on T-YSZ covered by 50 nm of  $\text{SiO}_2$  [28].

The structure and microstructure of the  $\text{LaFeO}_3$  thin film on T-YSZ was fully characterized by means of X rays diffraction and various electron microscopies (SEM, TEM and STEM-HAADF). Information about the stoichiometry of the films was obtained by local and line scan EDS analyses, as well as Raman spectroscopy.

## 2. Experimental procedure

3T-YSZ (3 %wt.  $\text{Y}_2\text{O}_3$ ) substrates 100 mm x 100 mm x 0,1 mm were purchased from Zircar Zirconia Inc. These sheets have a bending strength of 1 GPa. The corresponding radius of maximal curvature in case of pure bending can be calculated, considering a Young's modulus of 200 Gpa for 3T-YSZ [25]. For a thickness of 100  $\mu\text{m}$ , the bending radius is about 10 mm. The  $\text{LaFeO}_3$  thin films were deposited by Pulsed Laser Deposition using a Nd-YAG laser ( $\lambda=266\text{nm}$ ), the  $\text{LaFeO}_3$  target being purchased from Kurt Lesker Company. The deposition conditions were an oxygen pressure of 5,3 Pa (40 mTorr), an energy of laser of 90 mJ, a pulse frequency of 10 Hz, a duration of 4 ns, and a deposition time of 150 min. The distance between the target and the substrate was fixed at 70 mm. Two deposition temperatures, 750 °C and 850°C were used, but only the latter temperature led to crystallized  $\text{LaFeO}_3$ . Consequently, the results presented in this paper will focus on films deposited at 850°C.

The X-rays diffraction patterns were collected in grazing incidence ( $\lambda=1^\circ$ ) using a PANalytical EMPYREAN DY 1061 with a Cu  $K\alpha$  tube. Cell parameters were refined using the software Maud. The topography of the films was observed using a Scanning Electron Microscope Zeiss Supra 40, with an Inlens detector.

The samples for transmission electron microscopy (TEM) were prepared using a FIB ZEISS NEON 40EsB CrossBeam microscope. Conventional Transmission Electron Microscopy was performed on a TecnaiG2 ST equipped with a Si (Li) EDAX detector for X-Energy Dispersive Spectroscopy (EDS). More than 20 EDS local chemical analyses were acquired along the cross section of the layer, and the K factors for quantification of La and Fe were determined using the  $\text{LaFeO}_3$  target as standard. High resolution High Angle Annular Dark Field (HAADF)

images were acquired on a Titan cube G2, Cs corrected, operated at 300 kV, equipped with a Chemi STEM EDS system, allowing chemical elements line scans or mapping. Line scans with a step of one nm were realized from the substrate to the top of the layer, along the growth direction of the  $\text{LaFeO}_3$  grains, and parallel to the substrate, near the free surface and near the substrate, in order to gain information on the homogeneity of the  $\text{LaFeO}_3$  film.

The chemical composition was also investigated by Raman spectroscopy using a Horiba-Jobin-Yvon HR LabRAM HR800 Raman spectrometer, with two Ar ion laser wavelengths (488nm and 514nm). The acquisition parameters were a x50 long-working distance objective, 50% of 2mW laser power and an acquisition time of 5 minutes. The theoretical spatial resolution by  $R = 0.6 \cdot \lambda / NA$  (with  $NA=0.5$  and  $\lambda$  the used wavelength), and the spectral resolution is about  $1 \text{ cm}^{-1}$ .

### 3. Results and discussion

#### 3.1 Microstructure

The topography of  $\text{LaFeO}_3$ -850/T-YSZ thin film was investigated by SEM (Fig.1). The T-YSZ substrate presents a bumpy polycrystalline surface. Grains are ranging from 0.2 to 1  $\mu\text{m}$  in sizes and present smooth rounded terminations. The grains boundaries are clearly visible grain boundaries. After PLD deposition, SEM observations showed that the  $\text{LaFeO}_3$  layer covers the substrate without discontinuity — grains and grain boundaries alike — and follows the substrate texture. The presence of irregular droplets of  $\text{LaFeO}_3$  on the surface of the film (example encircled in Fig. 1) are well-known PLD artifacts and will not be discussed furthermore.

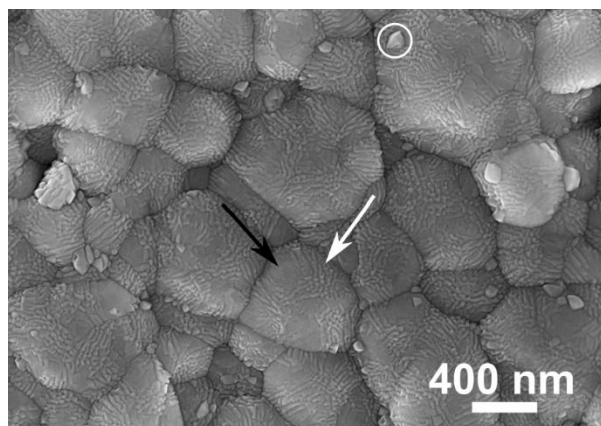


**Figure 1.** Topographic SEM image (SE) of  $\text{LaFeO}_3$ -850/T-YSZ. Arrows show the two typical types of surface texture present in the image. Encircled area shows a droplet i.e. a typical PLD artifacts.

The  $\text{LaFeO}_3$  film presents a similar nanostructuration than the one observed in previous work [14], with two distinctive areas. One area displays a rather smooth surface (black arrow on Fig. 1) that from experience can be associated with  $\text{LaFeO}_3$  grains with flat terminations. The

observation of the other area (white arrow on Fig. 1) shows a rougher surface with one privileged growth route, suggesting a compact juxtaposition of wall-like grains with pointy top terminations. It is interesting to note that the wall-like structures seem to be wrapped around the smooth areas. The shape of the smooth areas is not well defined although their analysis via the DigitalMicrograph software shows that in average the smooth areas present a major axis 37% longer than its minor axis; there is no preferential direction for major axis. The smooth areas cover 9% of the image which is significantly larger than the 6% we observed in a previous work [14]. Besides, our early work suggests that the proportion of smooth area is temperature dependent; the higher the temperature, the lower its proportion is. Hence, this discrepancy could be attributed to the much lower thermal conductivity of the T-YSZ substrate as compared to the thermal conductivity of silicon that was used as substrate in our early work, resulting in a lower effective surface temperature in the case of T-YSZ substrate. Indeed, the value of thermal conductivities for dense substrates at  $T=800\text{ }^{\circ}\text{C}$  are respectively  $\kappa=2,5\text{-}3\text{ W}\cdot\text{m}^{-1}\cdot\text{K}^{-1}$  for T-YSZ and  $\kappa= 30\text{-}40\text{ W}\cdot\text{m}^{-1}\cdot\text{K}^{-1}$  for Si single crystal [29,30].

The TEM cross sectional view in Fig. 2 shows a complete covering of the polycrystalline T-YSZ substrate, despite its bumpy nature. The  $\text{LaFeO}_3$  layer is 100 nm thick, with columnar grains starting from the substrate.

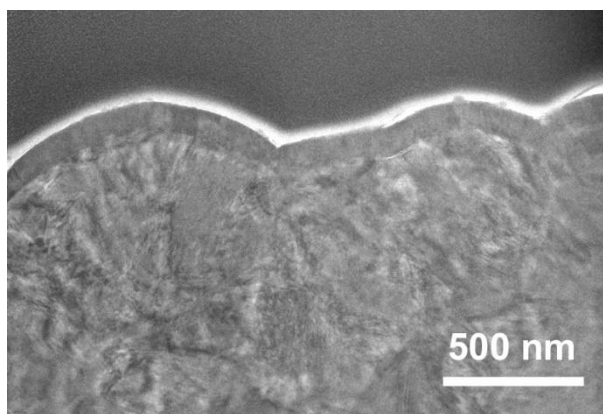


**Figure 2.** Cross sectional TEM view of a  $\text{LaFeO}_3\text{-850/T-YSZ}$  sample prepared by FIB.

### 3.2 Crystallographic structure

The  $\text{LaFeO}_3$  crystallographic structure is an orthorhombic deformation of the well-known cubic perovskite cell, linked to the tilting of  $\text{FeO}_6$  octahedra around the axes of the cubic cell and leading to a doubling of the cell parameter along one axis. Two settings are used in literature to describe the orthorhombic space group n° 62 of  $\text{LaFeO}_3$ , namely  $\text{Pbnm}$  and  $\text{Pnma}$ . We choose the former, for which the c-axis is the long axis of the unit cell. The experimental XDR pattern of the  $\text{LaFeO}_3$  thin film is shown in Fig. 3 (blue line), along with the calculated one

from refinement procedure (red line) and the difference between experimental and calculated pattern (green line). Peaks from the substrate are present along with the peaks for the LaFeO<sub>3</sub> phase. This indicates that the film thickness is smaller than the penetration depth of X rays in the case of grazing incidence with  $\alpha = 1^\circ$  around 90 nm [14]. Refinements of the cell parameters, crystallite size and strain and cation positions were pursued in the case of a two-phase system, the orthorhombic phase of LaFeO<sub>3</sub> (CIF file n° 1526450) and the tetragonal YSZ (CIF file n° 1521474). The background was fitted with a 5th order polynomial function and the peaks with pseudo-Voigt functions. Errors on cell parameters are  $2 \cdot 10^{-3}$  Å. The crystallite size is given with an error of 5 nm and strain with an error of  $2 \cdot 10^{-4}$ . The results concerning the LaFeO<sub>3</sub> phase are reported in Table 1 and 2.

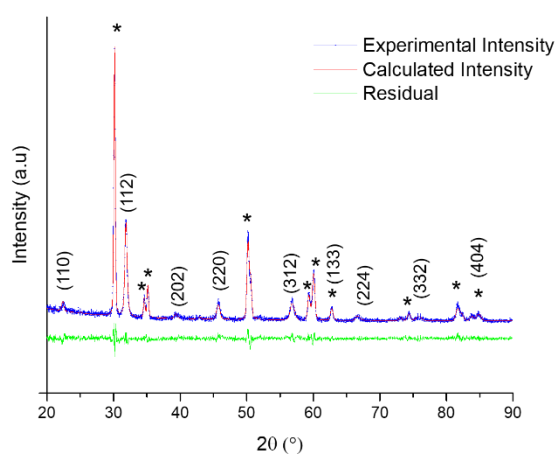


**Figure 3.** Experimental X-rays pattern of LaFeO<sub>3</sub> grown by PLD at 850°C on T-YSZ, along with the calculated pattern from Rietveld refinements and the difference between both diagrams. Peaks with an asterisk (\*) originate from the substrate.

**Table 1.**

Cell parameters, volume cell, crystallite size and refinement R factors on LaFeO<sub>3</sub> grown on T-YSZ, compared to results obtained for films grown on Si [14].

Sample	a (Å)	b (Å)	c (Å)	V (Å <sup>3</sup> )	Size (nm)	Strain	R <sub>exp</sub> / R <sub>wp</sub>
LaFeO <sub>3</sub> -850/T-YSZ	5.572	5.623	7.958	249.35	58	0.0025	11.4/14.3
LaFeO <sub>3</sub> -850/Si	5.539	5.613	7.912	245.99	52	0.0024	8.4/11.2
LaFeO <sub>3</sub> -750/Si	5.573	5.609	7.951	248.51	57	0.0022	11.1/13.1

Cell parameters, crystallite size and strain are much alike those obtained under the same deposition conditions on a silicon [100] substrate at a deposition temperature of 750°C instead of 850°C [14]. This can be linked to the much weaker thermal conductivity (k) of T-YSZ compared to Si [29,30]. It shows also that the thermal conductivity of substrate may influence

the cell parameters of thin films grown by PLD. Concerning the refined atomic positions (Table 2), let us recall that the orthorhombic perovskite structure of  $\text{LaFeO}_3$  (space group n°62) is built by the piling up of corner-linked  $\text{FeO}_6$  octahedra, tilted in opposite directions. The four oxygens noted  $\text{O}_2$  lay in the equatorial plane of the  $\text{FeO}_6$  octahedra as the two oxygens noted  $\text{O}_1$  correspond to the apex of the octahedron. As for the La cation, they occupy a body centered position with regards to the surrounding Fe cations and are coordinated to 12 oxygens (four  $\text{O}_1$  and eight  $\text{O}_2$ ). The refined atomic positions, obtained with an error of  $10^{-2}$  on oxygen positions and  $10^{-3}$  on La positions, are near those obtained for  $\text{LaFeO}_3$  grown on Si at  $750^\circ\text{C}$ , but differs from those given in [31, CIF file n° 1526450]. Fe-O bond lengths and O-Fe-O bond angles are a signature of the deformation of the  $\text{FeO}_6$  octahedra in the perovskite structure, so they were reported in Table 3.

**Table 2**

Refined atomic positions for  $\text{LaFeO}_3$ -850/T-YSZ compared to refined atomic positions obtained in literature.

	<b>LaFeO<sub>3</sub>-850/T-YSZ</b>			<b>LaFeO<sub>3</sub>-750/Si [14]</b>			<b>CIF n° 1526450 [31]</b>		
	x	y	z	x	y	z	x	y	z
Fe	0	0.5	0	0	0.5	0	0	0.5	0
La	0.999	0.012	0.25	0.002	0.022	0.25	0.993	0.0297	0.25
O <sub>1</sub>	0.057	0.445	0.25	0.061	0.467	0.25	0.080	0.485	0.25
O <sub>2</sub>	0.792	0.357	0.001	0.818	0.296	0.969	0.719	0.302	0.029

**Table 3.**

Bond lengths and bond angles for  $\text{LaFeO}_3$ -850/T-YSZ compared to data from literature.

<b>Sample</b>	<b>LaFeO<sub>3</sub>-850/T-YSZ</b>	<b>LaFeO<sub>3</sub>-750/Si [14]</b>	<b>CIF n° 1526450</b>
<b>Fe-O<sub>2</sub> (Å)</b>	2.584	2.442	2.0863
	2.584	2.442	2.0863
	1.410	1.548	1.9232
	1.410	1.548	1.9232
<b>Fe-O<sub>1</sub> (Å)</b>	2.039	2.025	2.0121
	2.039	2.025	2.0121
<b>O<sub>1</sub>-Fe-O<sub>2</sub> (°)</b>	77.7	73.46	86.80
	92.1	78.43	87.70
<b>O<sub>2</sub>-Fe-O<sub>2</sub> (°)</b>	85.7	89.3	88.60
	94.3	90.63	91.40



The deformation of the  $\text{FeO}_6$  octahedra in  $\text{LaFeO}_3$ -850/T-YSZ occurs mainly in the equatorial plane, as it is the case in  $\text{LaFeO}_3$ -750/Si. From the angle values, one can conclude that Fe cations are not at the center of octahedra equatorial planes. The distorted  $\text{FeO}_6$  octahedra deduced from Rietveld refinement of XRD patterns were drawn Fig. 4 for clarity.

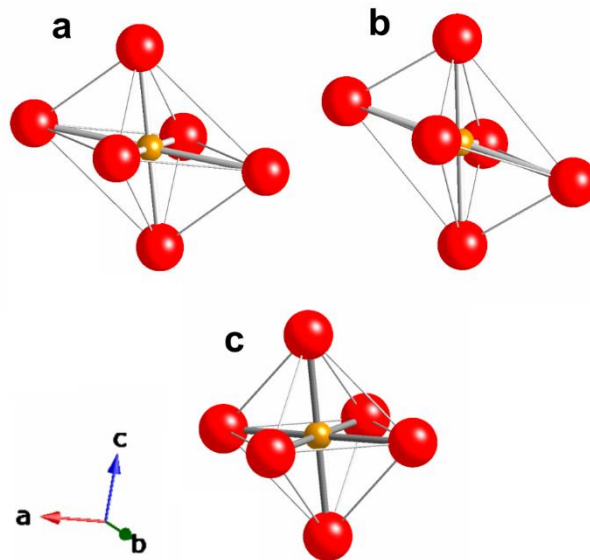


**Figure 4.**  $\text{FeO}_6$  octahedra deduced from Rietveld refinement, in case of  $\text{LaFeO}_3$ -850/T-YSZ,  $\text{LaFeO}_3$ -750/Si, and  $\text{LaFeO}_3$  [31, CIF file n° 1526450]

### 3.3 Chemical composition

The chemical composition of the  $\text{LaFeO}_3$ -850/T-YSZ thin film was investigated using different spectroscopies. Local EDS analyses (see Fig. 5a for a characteristic spectrum showing the peaks characteristic of La, Fe, as well as the Cu peaks due to TEM copper grid used) gave a mean cation composition of 53% La, 47 % Fe with a standard deviation of 2. It corresponds to the same mean composition that was measured for the  $\text{LaFeO}_3$ /Si thin films deposited under the same PLD conditions [14]. Several line scans were performed to reveal possible chemical composition fluctuations in the  $\text{LaFeO}_3$  layer. Line scans along the growth direction (Fig. 5b), or parallel to the substrate (Fig. 5c) always showed an iron deficiency in the layer composition. The fact that the iron under stoichiometry was more pronounced near the surface of the layer (Fig. 5b) may be attributed to a preferential thinning phenomenon. The cation composition of the layer is homogeneous from the substrate to the top of the layer, as well as along the layer, despite the observed composition variations, up to 10%. Indeed, these fluctuations occur between positions separated from 1 nm, so can unambiguously attributed to an acquisition phenomenon, and are not related to a real composition variation.

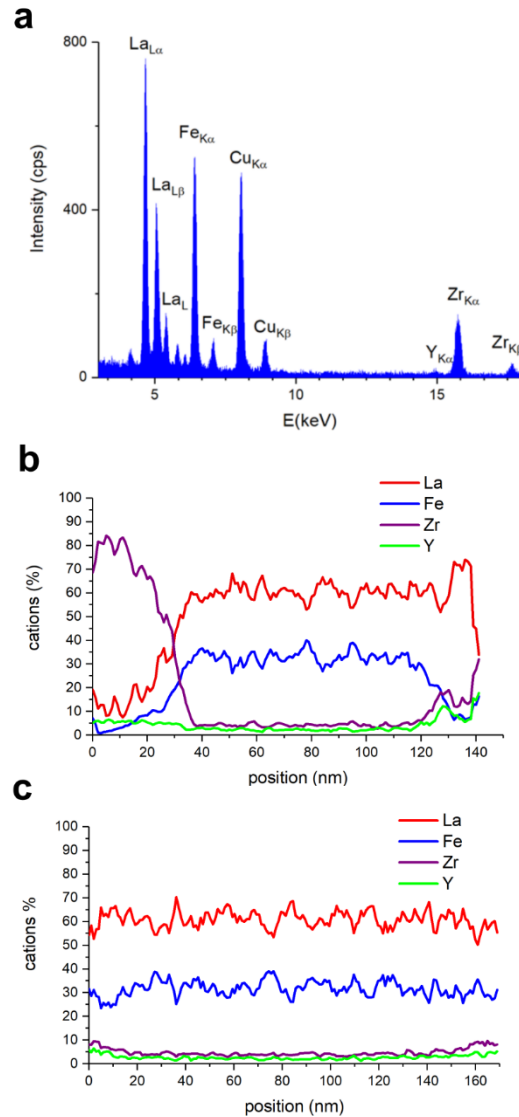


**Figure 5.** Energy dispersive spectroscopy. a) local EDS spectrum, showing the peaks characteristic of La and Fe, b) line scan from the substrate to the top of the LaFeO<sub>3</sub> layer, c) line scan in the LaFeO<sub>3</sub> layer perpendicular to the growth direction.

Raman spectroscopy (Fig. 6) was performed on the LaFeO<sub>3</sub>-850/T-YSZ sample as well as on the bare T-YSZ substrate; this later spectrum was subtracted from the LaFeO<sub>3</sub>-850/T-YSZ spectrum to remove the substrate contribution, using a renormalization factor [32]. Fig. 6a shows the raw spectra acquired at two different wavelengths in order to distinguish Raman peaks from the fluorescence ones. The data acquired with the 488nm wavelength (close to the LaFeO<sub>3</sub> absorption band range), led to the Raman spectrum presented in Fig. 6b (red line). This spectrum is in good agreement with the LaFeO<sub>3</sub>/SiO<sub>2</sub>/Si (100) thin film spectrum acquired with a laser wavelength of 488 nm [32] (blue line in Fig. 6b,) and the LaFeO<sub>3</sub> powder spectrum acquired with a laser wavelength of 514 nm [33] (yellow line in Fig. 6b).

The three series of peaks in the 100-200  $\text{cm}^{-1}$ , 250-350  $\text{cm}^{-1}$ , 400-450  $\text{cm}^{-1}$  ranges are the characteristic  $\text{LaFeO}_3$  first-order modes [34,35], and the peaks in range 1100-1400  $\text{cm}^{-1}$  correspond to second order modes [33]. According to first-principles calculations [36] and Raman measurements under temperature-controlled hydration [37], the peak detected at 620-680  $\text{cm}^{-1}$  is a signature of vacancies in the  $\text{LaFeO}_3$  layer, in agreement with the EDS analyses.

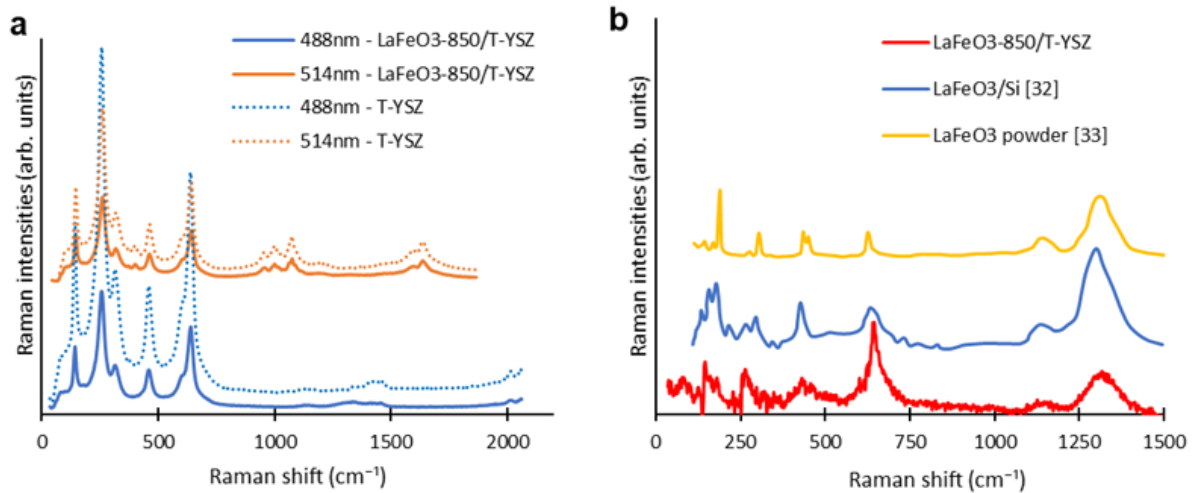


**Figure 6.** Raman spectroscopy a) Raw spectra of  $\text{LaFeO}_3$ -850/T-YSZ (straight lines) and of the T-YSZ substrate (dot lines) using two different wavelengths (488 nm blue lines and 514 nm orange lines) b) Raman spectrum of the  $\text{LaFeO}_3$  layer (red line) deduced from the raw data, compared to Raman spectra of  $\text{LaFeO}_3$  thin film deposited on Si(100) [32] (blue line) and of  $\text{LaFeO}_3$  powder (yellow line) [33].

### 3.4 Atomic-scale microstructure of the $\text{LaFeO}_3$ thin films

STEM-HAADF imaging of the  $\text{LaFeO}_3$  layer was performed to investigate the microstructure of grains, in particular their growth direction as well as exposed facets, but also to gain information on the curvature accommodation.

Bunches of  $\text{LaFeO}_3$  grains with the same zone axis were grown whatever the curvature of the substrate, as can be seen in Fig. 7 and Fig. 8. High resolution STEM HAADF allowed to image the La and Fe cations columns (insert in Fig. 7). The two FFT inserts in Fig. 7, carried out on two adjacent grains, in the region where the curvature of the substrate is at his maximum, show two variants oriented at  $90^\circ$ , with the same zone axis [1-10]. In one case, the growth direction is along the [110] axis, and in the other case, along [010]. Let us remind that these orientations correspond respectively to  $[001]_c$  and  $[100]_c$  of the pseudo perovskite cubic cell. This type of domains is quite common in  $\text{LaFeO}_3$  and are known to be separated by {112} twins [38]. Such twins were not observed in  $\text{LaFeO}_3$  thin films grow on Si [14] and can be related to an

adaptation of the curvature of the T-YSZ substrate. The terminations of the grains are rather flat, with  $\{110\}$  or  $\{010\}$  exposed facets. In regions with minor curvature of the substrate, (right part of Fig.7) one observes a tilt of a few degrees between two adjacent grains.

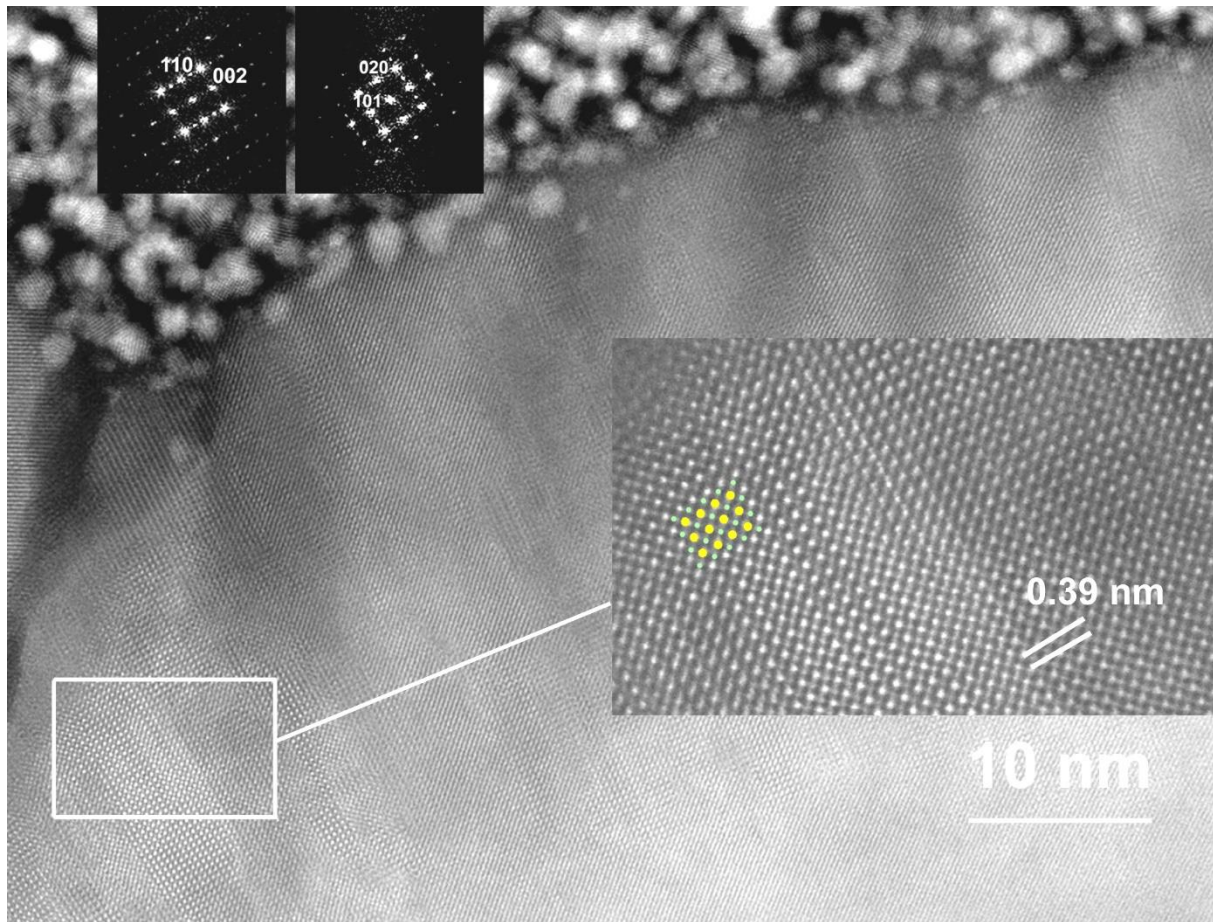


**Figure 7.** STEM-HAADF image of  $\text{LaFeO}_3\text{-850/T-YSZ}$  in a highly curved region. The chemical contrast allows to image columns of La and Fe cations. The projected structure is superimposed in the insert (La in yellow and Fe in green).

Tip-like termination for  $\text{LaFeO}_3$  grains were also observed (see Fig.8). In that case, the growth direction is  $[110]$  and the exposed facets  $\{010\}$  or  $\{100\}$ .

If one compares the exposed facets and shapes of the  $\text{LaFeO}_3$  grains grown on T-YSZ with those grown on Si [14], it appears that tip-like or flat-ended terminations are the privileged shapes for  $\text{LaFeO}_3$  grains grown by PLD, whatever the substrate. From the comparison, one can also conclude that the  $[110]$  and  $[010]$  are the two main growth directions. However, the link between shape of the grain termination and exposed facets is not the same. For tip-like grain terminations, the exposed facets are  $\{010\}$  and  $\{100\}$  with a  $[110]$  growth direction for

LaFeO<sub>3</sub>-850/T-YSZ, as for LaFeO<sub>3</sub>-850/Si, the exposed facets are {110} and {-110} with a [010] growth direction [14]. In terms of pseudo cubic perovskites cell, this means that the LaFeO<sub>3</sub> grown on T-YSZ substrate grains exposed mainly flat {010}<sub>c</sub> facets and tip-like {110}<sub>c</sub> facets.

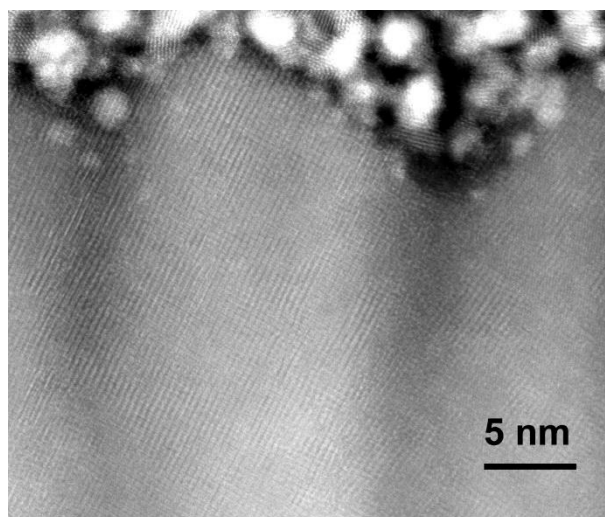


**Figure 8.** STEM-HAADF image of LaFeO<sub>3</sub>-850/T-YSZ grains oriented with a [001] zone axis, showing tip like terminations of LaFeO<sub>3</sub> grains.

## Conclusion

## References

- [1] M. Pidburtnyi, B. Zanca, C. Coppex, S. Jimenez-Villegas, V. Thangadurai, A Review on Perovskite-Type LaFeO<sub>3</sub> Based Electrodes for CO<sub>2</sub> Reduction in Solid Oxide Electrolysis Cells: Current Understanding of Structure–Functional Property Relationships, *Chem. Mater.* 33 (2021) 4249–4268. <https://doi.org/10.1021/acs.chemmater.1c00771>
- [2] X. Dai, Ch. Yu, Q. Wu, Comparison of LaFeO<sub>3</sub>, La<sub>0.8</sub>Sr<sub>0.2</sub>FeO<sub>3</sub>, and La<sub>0.8</sub>Sr<sub>0.2</sub>Fe<sub>0.9</sub>Co<sub>0.1</sub>O<sub>3</sub> perovskite oxides as oxygen carrier for partial oxidation of methane, *J. of Natural Gas Chem.* 17 (2008) 415–418. [https://doi.org/10.1016/S1003-9953\(09\)60019-0](https://doi.org/10.1016/S1003-9953(09)60019-0)
- [3] S. Tasleem, M. Tahir, Recent progress in structural development and band engineering of perovskites materials for photocatalytic solar hydrogen production: A review, *Int. J. of Hydrogen Energy* 45 (2020) 19078 -19111. <https://doi.org/10.1016/j.ijhydene.2020.05.090>
- [4] M. Humayun, H. Ullah, M. Usman, A. Habibi-Yangjeh, A. A. Tahir, Ch. Wang, W. Luo, Perovskite-type lanthanum ferrite based photocatalysts: Preparation, properties, and applications, *J. of Ener. Chem.* 66 (2022) 314–338. <https://doi.org/10.1016/j.jechem.2021.08.023>
- [5] F. Andrei, I. Boerasu, R. Birjega, A. Moldovan, M. Dinescu, V. Ion, C. Mihailescu, N. D. Scarisoreanu, V. Leca, The effects of the oxygen content on the photoelectrochemical

- properties of LaFeO<sub>3</sub> perovskite thin films obtained by pulsed laser deposition, *App. Phys. A* 125 (2019) 807. <https://doi.org/10.1007/s00339-019-3089-4>
- [6] M.V.N.S. Gupta, H. Baig, K.S. Reddy, T.K. Mallick, B. Pesala, A.A. Tahir, Photoelectrochemical Water Splitting Using a Concentrated Solar Flux-Assisted LaFeO<sub>3</sub> Photocathode, *ACS Appl. Energy Mater.* 3 (2020) 9002–9009. <https://dx.doi.org/10.1021/acsaem.0c01428>
- [7] N.D. Tho, D.V. Huong, P.Q. Ngan, G.H. Thai, D.T.A. Thu, D.T. Thu, N. Thi, M. Tuoi, N.N. Toan, H.T. Giang, Effect of sintering temperature of mixed potential sensor Pt/YSZ/LaFeO<sub>3</sub> on gas sensing performance, *Sens. and Actuat. B* 224 (2016) 747–754. <http://dx.doi.org/10.1016/j.snb.2015.10.113>
- [8] S. Thirumalairajan, K. Girija, Valmor R. Mastelaro, N. Ponpandian, Surface morphology-dependent room-temperature LaFeO<sub>3</sub> nanostructure thin films as selective NO<sub>2</sub> gas sensor prepared by radio frequency magnetron sputtering, *ACS Appl. Mater. Interf.* 6 (2014) 13917–13927. <https://dx.doi.org/10.1021/am503318y>
- [9] A.A. Alharbi, A. Sackmann, U. Weimar, N. Barsan, Essential role of electrode materials in ethylene and acetylene sensing selectivity for LaFeO<sub>3</sub> based gas sensors, *Sens. and Act. B* 353 (2022) 131079. <https://doi.org/10.1016/j.snb.2021.131079>
- [10] J. Hu, X. Chen, Y. Zhang, Batch fabrication of formaldehyde sensors based on LaFeO<sub>3</sub> thin film with ppb-level detection limit, *Sens. and Act. B* 349 (2021) 130738. <https://doi.org/10.1016/j.snb.2021.130738>
- [11] K.J. May, D. P. Fenning, T. Ming, W. T. Hong, D. Lee, K. A. Stoerzinger, M. D. Biegalski, A. M. Kolpak, Y. Shao-Horn, Thickness-Dependent Photoelectrochemical Water Splitting on Ultrathin LaFeO<sub>3</sub> Films Grown on Nb:SrTiO<sub>3</sub>, *J. Phys. Chem. Lett.* 6 (2015) 977–985. <http://dx.doi.org/10.1021/acs.jpcclett.5b00169>
- [12] Y.H. Lee, J.M. Wu, Epitaxial growth of LaFeO<sub>3</sub> thin films by RF magnetron sputtering, *J. of Crys. Grow.* 263 (2004) 436–441. <http://dx.doi.org/10.1016/j.jcrysgro.2003.12.007>
- [13] J. Park, Y. Kim, D. Lee, J.H. Song, J.H. Park, Twin-free Epitaxial LaFeO<sub>3</sub> Films Grown on Orthorhombic GdScO<sub>3</sub>(110)<sub>o</sub> Substrates, *J. of the Kor. Phys. Soc.*, 76 ( 2020) 273-276. <http://dx.doi.org/10.3938/jkps.76.273>
- [14] M. Jedrusik, Ch. Turquat, L. Cieniek, A. Kopia, Ch. Leroux, Nanostructured LaFeO<sub>3</sub>/Si thin films grown by pulsed laser deposition, *Eur. Phys. J. Appl. Phys.* 96 (2021) 30301. <https://doi.org/10.1051/epjap/2021210195>
- [15] E. Haye, F. Capon, S. Barrat, P. Boulet, E. André, C. Carteret, S. Bruyere, Properties of rare-earth orthoferrites perovskite driven by steric hindrance, *J. of All. and Comp.* 657 (2016) 631-638. <https://doi.org/10.1016/j.jallcom.2015.10.135>
- [16] N. Mahato, A. Banerjee, A. Gupta, S. Omar, K. Balani, Progress in material selection for solid oxide fuel cell technology: A review, *Prog. in Mat. Sci.* 72 (2015) 141–337. <http://dx.doi.org/10.1016/j.pmatsci.2015.01.001>
- [17] J.W. Yoon, E. Di Bartolomeo, E. Traversa, NO<sub>2</sub> adsorption behaviour on LaFeO<sub>3</sub> electrodes of YSZ-based non-nernstian electrochemical sensors, *J Electroceram.* 26 (2011) 28–31. <http://dx.doi.org/10.1007/s10832-010-9623-6>
- [18] T. Ueda, M. Sakai, K. Kamada, T. Hyodo, Y. Shimizu, Effects of composition and structure of sensing electrode on NO<sub>2</sub> sensing properties of mixed potential-type YSZ-based gas sensors, *Sens. and Act. B* 237 (2016) 247-255. <http://dx.doi.org/10.1016/j.snb.2016.06.103>
- [19] D. Corzo, G. Tostado-Blázquez, D. Baran, Flexible Electronics: Status, Challenges and Opportunities, *Front. in Electr.* 1 (2020) 594003. <http://dx.doi.org/10.3389/felec.2020.594003>
- [20] P. Kum-onsa and P. Thongbai, Dielectric properties of poly(vinylidene fluoride)-based nanocomposites containing a LaFeO<sub>3</sub> nanoparticle filler, *J Mater Sci: Mater Electron.* 32 (2021) 13985–13993. <https://doi.org/10.1007/s10854-021-05974-8>
- [21] M. Wu, Z. Jiang, X. Lou, F. Zhang, D. Song, S. Ning, M. Guo, S. J. Pennycook, J.Y. Dai, Z. Wen, Flexoelectric Thin-Film Photodetectors, *Nano Lett.* 21 (2021) 2946–2952. <https://doi.org/10.1021/acs.nanolett.1c00055>

- [22] S.J. Chen, S. Patel, E. Narumi, D. T. Shaw, D.St. Julien, T.D. Ketcham, BSCCO-2212 thick films on a flexible YSZ substrate, *Physica C* 218 (1993) 191-196. [https://doi.org/10.1016/0921-4534\(93\)90282-U](https://doi.org/10.1016/0921-4534(93)90282-U)
- [23] R. Aggarwal, C. Jin, P. Pant, J. Narayan, and R. J. Narayan, Growth of biepitaxial zinc oxide thin films on silicon (100) using yttria-stabilized zirconia buffer layer, *Appl. Phys. Lett.* 93 (2008) 251905. <https://doi.org/10.1063/1.3050529>
- [24] K. K. Gopalan, D. Rodrigo, B; Paulillo, K. K. Soni, and V. Pruneri, Ultrathin Yttria-Stabilized Zirconia as a Flexible and Stable Substrate for Infrared Nano-Optics, *Adv. Optical Mater.* 7 (2019) 1800966, <https://dx.doi.org/10.1002/adom.201800966>
- [25] P. Stastny, Z. Chlup, P. Roupčová, M. Trunec, Thin high-strength zirconia tapes with extreme flexibility, *J. of Asian Cer. Soci.* 9 (2021) 964-974. <https://dx.doi.org/10.1080/21870764.2021.1930744>
- [26] S. Singh, M. Yarali, S. Shervin, V. Venkateswaran, K. Olenick, J. A. Olenick, J.H. Ryou, A. Mavrokefalos, Temperature-dependent thermal conductivity of flexible yttria-stabilized zirconia substrate via 3w technique, *Phys. Status Solidi A* 214 (2017) 1700069. <https://dx.doi.org/10.1002/pssa.201700069>
- [27] S. Chen, D. Gu, Y. Zheng, H. Chen, L. Guo, Enhanced performance of NiO–3YSZ planar anode-supported SOFC with an anode functional layer, *J Mater Sci* 55 (2020) 88–98. <https://doi.org/10.1007/s10853-019-04007-4>
- [28] Y. Zheng, Ch. Yuan, S. Wei, H. Kim, F. Yao, J.H. Seo, Direct Growth of two dimensional molybdenum disulfide on flexible ceramic substrate, *Nanomaterials* 9 (2019) 1456. <https://www.mdpi.com/2079-4991/9/10/1456>
- [29] K. W. Schlichting, N. P. Padture, P. G. Klemens, Thermal conductivity of dense and porous yttria-stabilized zirconia, *J. of Mater. Sci.* 36 (2001) 3003-3010. <https://doi.org/10.1023/A%3A1017970924312>
- [30] Shujuan Li, Xincheng Yin, Zhen Jia, Zhipeng Li & Lili Han Modeling of plasma temperature distribution during micro-EDM for silicon single crystal, *The Inter. J. of Advanc. Manuf. Tech.* **107**, (2020) 1731–1739. <https://doi.org/10.1007/s00170-020-05135-x>
- [31] L. Sangaletti, L.E. Depero, B. Allieri, P. Nunziante, E. Traversa, An X-ray study of the trimetallic  $\text{La}_x\text{Sm}_{1-x}\text{FeO}_3$  orthoferrites, *J. of the Eur. Ceram. Soc.* 21 (2001) 719-726. [https://doi.org/10.1016/S0955-2219\(00\)00267-3](https://doi.org/10.1016/S0955-2219(00)00267-3)
- [32] S. Nandi, D. Blanck, T. Carlier, M.-H. Chambrier, A.-S. Mamede, M. Trentesaux, P. Simon, N. Nuns, P. Roussel, A. Ferri, J.-F. Paul and E. Berrier,  $\text{LaFeO}_3$  thin films as relevant models for the surface investigation of 3-way catalysts, *Surf. and Interf. Anal.* 50 (2018) 1018-1024. <https://doi.org/10.1002/sia.6450>
- [33] J. Bielecki, P. Svedlindh, D. T. Tibebe, S. Cai, S.-G. Eriksson, L. Börjesson and C. S. Knee, Structural and magnetic properties of isovalently substituted multiferroic  $\text{BiFeO}_3$ : Insights from Raman spectroscopy, *Phys. Rev. B* 86 (2012) 184422. <https://doi.org/10.1103/PhysRevB.86.184422>
- [34] B. Jiang, L. Li, Q. Zhang, J. Ma, H. Zhang, K. Yu, Z. Bian, X. Zhang, X. Ma, D. Tang, Iron–oxygen covalency in perovskites to dominate syngas yield in chemical looping partial oxidation, *J. of Mater. Chem. A* 9 (2021) 13008-13018. <https://doi.org/10.1039/D1TA02103F>
- [35] A. P. B. Selvadurai, V. Pazhanivelu, C. Jagadeeshwaran, R. Murugaraj, I. P. Muthuselvam and F. C. Chou, Influence of Cr substitution on structural, magnetic and electrical conductivity spectra of  $\text{LaFeO}_3$ , *J. of All. and Comp.* 646 (2015) 924-931. <http://dx.doi.org/10.1016/j.jallcom.2015.05.213>
- [36] P. Eyméoud, Ch. Turquat, C. Pardanaud, Ch. Leroux and A. Merlen, submitted 2022.
- [37] D. Blanck, A. Schön, A.-S. Mamede, C. Dujardin, J.-P. Dacquain, P. Granger, J.-F. Paul, E. Berrier, In situ Raman spectroscopy evidence of an accessible phase potentially involved in the enhanced activity of La-deficient lanthanum orthoferrite in 3-way catalysis (TWC), *Catalysis Today* 283 (2017) 151-157. <https://doi.org/10.1016/j.cattod.2016.03.045>

[38] W.L. Wang, H.Y. Lu, Phase-Transformation-Induced Twinning in Orthorhombic  $\text{LaGaO}_3$ : {121} and [010] Twins, J. Am. Ceram. Soc. 89 (2006) 281–291. <https://dx.doi.org/10.1111/j.1551-2916.2005.00673.x>

### **Acknowledgments :**

This work was realized with a Ph.D. scholarship of the French embassy in Poland. The TEM research has received funding from the European Union's Horizon 2020 research and innovation program under Grant agreement ESTEEM3. Authors would like to thank C. Pardanaud for fruitful discussions.